An Integrated Geometrical and Stochastic Approach For Accurate Infant Brain Extraction

Amir Alansary, et al.

ICIP, 2014

NeuroSpectrum Insights, Inc.
info@neurospectruminsights.com
www.neurospectruminsights.com

AN INTEGRATED GEOMETRICAL AND STOCHASTIC APPROACH FOR ACCURATE INFANT BRAIN EXTRACTION

A. Alansary[1], *A. Soliman*[1], *M. Nitzken*[1], *F. Khalifa*[1], *A. Elnakib*[1], *M. Mostapha*[1], *M. F. Casanova*[2], *and A. El-Baz*[1] *

[1]BioImaging Laboratory, Bioengineering Department,University of Louisville, Louisville, KY, USA.

[2]Department of of Psychiatry and Behavioral Science, University of Louisville, Louisville, KY, USA

ABSTRACT

This paper presents a novel approach for extracting the brain from 3D T1-weighted MR images. The proposed approach combines a stochastic two-level Markov-Gibbs random field (MGRF) image model with a geometric model that parcels the brain into a set of nested iso-surfaces using a fast marching level setmethod. The classification of each brain voxel found on the iso-surfaces is performed based on the first-order (a linear combination of discrete gaussian (LCDG) model) and second-order (an MGRF model with analytically estimated parameters) visual appearance features of the brain structures. Our approach is tested on 280 infant 3D MR brain scans and evaluated on 9 data sets using the Dice coefficient, the 95-percentile modified Hausdorff distance, and absolute brain volume difference. Experimental results showed that the fusion of the stochastic and geometric models of brain MRI data has led to more accurate brain extraction, when compared with other widely-used brain extraction tools, such as BET, BET2, and brain surface extractor (BSE).

Index Terms— Brain extraction, skull stripping, MRI, MRFs, BET, Iso-surfaces, infant

1. INTRODUCTION

Brain extraction is the process of removing all the outer tissues (e.g. eyes, dura, scalp, and skull) around the brain which consists of the gray matter (GM) and white matter (WM), while the inclusion of cerebrospinal fluid (CSF) in the brain depends on the application. Brain extraction is a primary step in neuroimaging analysis as well as a pre-processing step for many brain analysis algorithms like intensity normalization, registration, classification, and segmentation. Accordingly, accurate brain extraction is crucial for these algorithms to work properly. For instance, in cortical thickness estimation, inaccurate skull stripping (e.g. failing to remove the dura or missing brain parts) can result in an overestimation or underestimation of the cortical thickness [1].

Many brain extraction approaches are designed to work on T1-weighted MR brain images. These methods use different techniques, such as, deformable models, atlas-based and label fusion, and hybrid algorithms. For deformable model approaches, Smith [2] developed an automated method, which is widely known as brain extraction tool (BET), where the deformable contour is guided by a set of locally adaptive forces, which include morphological and image-based terms in addition to a surface smoothness constraint. Liu et al. [3] presented another automated brain extraction method using a deformable model based on a set of Wendland's radial basis functions. Also, Zhuang et al. [4] used a model-based level set based on two forces: the mean curvature of the curve and the intensity characteristics of the cortex in MR images. For atlas-based and label fusion approaches, Ashburner and Friston [5] used a voxel-based morphometry which involves a voxel-wise comparison of the local concentration of gray matter between two groups of subjects. Leung et al. [6] presented a multi-atlas propagation and segmentation method using a template library-based segmentation technique. For hybrid approaches, Iglesias et al. [7] developed a learning-based brain extraction system which combines two models: a discriminative model based on a random forest classifier trained to detect the brain boundary and a generative model based on finding the contour with highest likelihood according to the discriminative model which is refined later using graph cuts. Segonne et al. [8] presented a hybrid approach that combined watershed algorithms and deformable surface models. Rex et al. [9] developed a meta-algorithm that executes many brain extraction algorithms and a registration procedure followed by an approach to combine the results.

In summary, different brain extraction approaches have been developed; however, the existing approaches have their

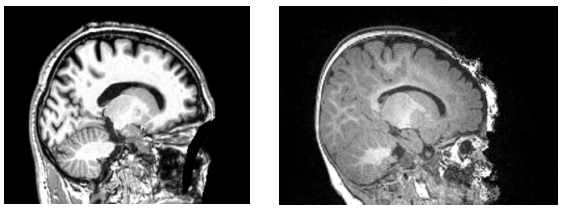

(a) (b)

Fig. 1. T1-weighted MRI for (a) adult and (b) infant brains.

*Corresponding author:- Tel:(502)-852-5092, Fax:(502)-852-6806, E-mail: aselba01@louisville.edu

own drawbacks. Some of them give better results when removing non-brain tissue while losing some brain parts, and others give better results when extracting the whole brain while keeping some non-brain tissue parts [10, 11]. Atlas-based approaches are very time consuming and their performance heavily depends on the registration accuracy and the spatial correspondence between the atlas and the test subject, in addition to the difficulty of constructing an infant brain atlas [12]. The majority of the existing techniques are developed to work for adult MR brain images and fail to accurately extract the brain from MR infant images due to the reduced contrast and higher noise [13] (see Fig. 1).

To overcome the mentioned limitations, we present a hybrid framework that possesses the ability to accurately extract brain tissue from infant MR brain images. The proposed framework integrates both stochastic and geometric approaches and consists of four basic steps: (i) bias correction, (ii) skull stripping, and (iii) final brain extraction using an iso-surfaces approach guided by a joint joint Markov-Gibbs random field (MGRF) model image model that integrates the visual appearance features of the MR brain images. Details of our framework are described in the following section.

2. BIAS CORRECTION

Illumination non-uniformity of infant brain MRIs, which is known as bias field, limits the accuracy of the existing brain extraction approaches. Therefore, to accurately extract the brain, it is important to account for the low frequency intensity non-uniformity or inhomogeneity. In this work, we used the generalized Gauss-Markov random field (GGMRF) model [14, 15] that is applied after brain intensity normalization using the nonparametric approach proposed in [16]. This step accounts for illumination non-uniformity and noise effects and removes (smooth) inconsistencies of the brain MR images by accounting for the spatially homogeneous 3D pairwise interactions between the gray levels of the MR data. Namely, the gray level values $q \in \mathbf{Q} = \{0, \ldots, Q-1\}$ are considered as samples from a 3D GGMRF model [14, 15] of measurements with the voxel 26-neighborhors. The continuity of q values of each brain MR scan is amplified by using their maximum A posteriori (MAP) estimates [14, 15] and voxel-wise stochastic relaxation (iterative conditional mode (ICM) [17]):

$$\widehat{q}_s = \arg\min_{\widetilde{q}_s} \left[|q_s - \widetilde{q}_s|^{\alpha} + \rho^{\alpha} \lambda^{\beta} \sum_{r \in \nu_s} \eta_{s,r} \, |\widetilde{q}_s - q_r|^{\beta} \right] \quad (1)$$

where q_s and $\widetilde{q}_s$ denote the original gray level values and their expected estimates, respectively, at the observed 3D location, $s = (x, y, z)$; ν_s is the 26-neighborhood voxel set; $\eta_{s,r}$ is the GGMRF potential, and ρ and λ are scaling factors. The parameter $\beta \in [1.01, 2.0]$ controls the level of smoothing (e.g., $\beta = 2$ for smooth vs. $\beta = 1.01$ for relatively abrupt edges). The parameter $\alpha \in \{1, 2\}$ determines the Gaussian, $\alpha = 2$, or Laplace, $\alpha = 1$, prior distribution of the estimator. To demonstrate the effect of the first step of the proposed framework, an example of the original, and bias-corrected (intensity normalization and GGMRF edge preservation) brain MR data is shown in Fig. 2 (a), (b), and (c), respectively.

3. SKULL STRIPPING

The second step of the proposed framework after bias correction is to remove the non-brain tissue from the MR images. To accomplish this, we used the BET [2], which uses a deformable model-based approach to remove the skull from MR brain images. [2]. The initial brain extraction result of Fig. 2 (c) after the BET is shown in Fig. 2 (d). While, the BET extracted the whole brain without losing any brain parts, it fails to remove all non-brain tissues (parts of the skull and the extra-cranial tissues are classified as brain tissue). For some clinical applications, such as cortical thickness measurement, inaccurate skull stripping results in an over- or under-estimation of the thickness. Therefore, it is important to account for the inaccurate skull stripping results after the BET step.

4. VISUAL APPEARANCE-GUIDED ISO-SURFACES

In order to obtain more accurate brain extraction results, we propose an additional processing step based on the geometric features of the brain to account for BET's skull stripping errors. Since the non-brain tissues are brighter than brain tissue, this step exploits the visual appearance features of the MR brain data. Namely, an evolving iso-surfaces-based approach is proposed to remove the non-brain tissues, which is guided by the visual appearance features of the MR data. First, a set of nested, tangent surfaces (i.e., iso-surfaces) are generated by the fast marching level set (FMLS) approach [18], using the extracted brain from the BET step. In order to accurately classify MRI voxels as brain or non-brain, we need to accurately model MR data visual appearance. To achieve this goal, we will use a joint MGRF model image model, where the 3D T1-weighted MR brain images, $\mathbf{g}$, and its region map, $\mathbf{m}$, are described with the following joint probability model:

$$P(\mathbf{g}, \mathbf{m}) = P(\mathbf{g}|\mathbf{m}) P(\mathbf{m}) \quad (2)$$

where $P(\mathbf{m})$ is an unconditional probability distribution of maps, and $P(\mathbf{g}|\mathbf{m})$ is a conditional distribution of the images given the map. The ultimate goal is to accurately estimate $P(\mathbf{g}|\mathbf{m})$ and $P(\mathbf{m})$, which are described next.

First-order visual appearance ($P(\mathbf{g}|\mathbf{m})$): To accurately approximate the marginal probability distributions of the brain and non-brain tissue, the empirical gray level distribution of a given $\mathbf{g}$ distribution is precisely approximated with a linear combination of discrete Gaussians (LCDG) with positive and negative components [19–21]. The LCDG restores brain and non-brain transitions more accurately than a conventional

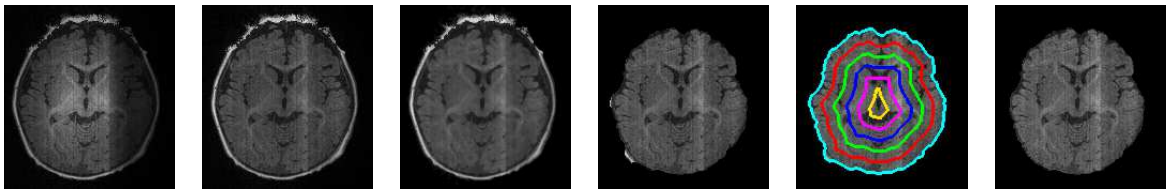

(a) (b) (c) (d) (e) (f)

Fig. 2. Step-wise brain extraction using the proposed framework: (a) the original MR image, (b) the bias-corrected image, (c) the GGMRF-smoothed image obtained with $\rho = 1$, $\lambda = 5$, $\beta = 1.01$, $\alpha = 2$, and $\eta_{s,r} = \sqrt{2}$, (d) the extracted brain using BET [2], (e) the iso-surfaces used to remove non-brain tissues, and (f) the final extracted brain.

mixture of only positive Gaussians, thus yielding a better initial brain map ($\mathbf{m}$) formed by voxel-wise classification of the image gray values.

Second-order visual appearance ($P(\mathbf{m})$): In order to overcome noise effect and to ensure the homogeneity of the segmentation, the spatial voxel interactions between the region labels of a given brain map $\mathbf{m}$ are also taken into account using the popular Potts MGRF model. Let $\mathbf{R}$ and $f_{a,\text{eq}}(\mathbf{m})$ denote a 3D arithmetic lattice that supports $\mathbf{g}$ and $\mathbf{m}$, and the relative frequency of the equal label pairs in the equivalent voxel pairs $\{((x,y,z),(x+\xi,y+\zeta,z+\kappa)):\ (x,y,z) \in \mathbf{R};\ (x+\xi,y+\zeta,z+\kappa) \in \mathbf{R};\ (\xi,\zeta,\kappa) \in \nu_s$. The initial region map $\mathbf{m}$ results in approximate analytical maximum likelihood estimates of the potentials [22, 23]: $v_{\text{eq}} = -v_{\text{ne}} \approx 2f_{\text{eq}}(\mathbf{m}) - 1$; which allow for computing the voxel-wise MGRF probabilities $p_{x,y,z}(m_{x,y,z} = \lambda)$ of each brain label; $\lambda \in \mathbf{L} = \{\text{“brain”}, \text{“non-brain”}\}$ [24, 25]. In total, Algorithm 1 summarizes the basic steps of the proposed framework for brain extraction.

Algorithm 1 Proposed brain extraction approach

1 Correct the bias of the MR brain data.
   (a) Brain intensity normalization [16].
   (b) GGMRF edge preservation [14, 15].
2 Strip the skull using BET [2].
3 Estimate the LCDG models for the brain and non-brain tissues using the results in Step 2.
4 Form an initial map $\mathbf{m}$ by voxel-wise classification using the LCDG models found in Step 3
5 Estimate analytically the Gibbs potentials for the pair-wise MGRF model of $\mathbf{m}$ to identify the MGRF probability.
6 Calculate the distance map (Fig. 2 (e)) inside the binary mask obtained from BET using FMLS [18].
7 Generate a set of N nested, tangent iso-surfaces (Fig. 2 (e)) using the distance map calculated in Step 6.
8 while $j \leq N$
   (a) Select the j^{th} iso-surfacer and classify its voxels using a Bayes classifier combining the first and second-order visual appearance features.
   (b) Are all the voxels on the selected iso-surfaces classified only as brain tissue?
      • No $\longrightarrow$ **Go to Step 8 (a)**.
      • Yes $\longrightarrow$ **Break**
9 Apply connected component analysis and 3×3×3 median filtering to obtain the final results.

5. EXPERIMENTAL RESULTS AND CONCLUSIONS

To measure the robustness and performance of our approach, we applied our method to 280 T1-weighted MR infant brain data sets which were obtained from the Infant Brain Imaging Study (IBIS) [26], and evaluated using 9 data sets with known manually segmented ground truth that were obtained by an MR expert. MR data was acquired at 3T and consists of T1- and T2-weighted MR images of infants scanned at approximately 6 months old with voxel size of $1\times1\times1$ mm^3.

A step-wise brain extraction using the proposed approach for a selected axial cross-section of one subject is demonstrated in Fig. 2. The input MR image (Fig. 2(a)) is first bias corrected (intensity normalized Fig. 2 (b)) and GGMRF [14, 15] edge preservation (Fig. 2 (c)). This is followed by an initial brain extraction using BET [2] (Fig. 2 (d)). Then, the proposed iso-surfaces based approach is employed to achieve the final segmentation as shown in Fig. 2 (f). It is clear from the results in Fig. 2 that the proposed framework provides more accurate infant brain extraction than BET.

The performance of the proposed framework was evaluated using three performance metrics: (*i*) the Dice similarity coefficient (DSC) [27], (*ii*) 95-percentile modified Hausdorff distance (MHD) [28], and (*iii*) absolute brain volume difference (ABVD). All metrics were obtained by comparing brain extraction results against the 9 data sets with available ground truth segmentation. As demonstrated in Table 1, the mean DSC, MHD, and ABVD values for our automated segmentation of the whole brain are 95.86±0.77%, 6.32±2.26 mm, and 3.76±2.52%, respectively. This confirms the high accuracy of the proposed segmentation technique.

To highlight the advantage of the proposed framework we compared its performance to three widely-used brain extraction tools: the brain surface extractor (BSE) [29], BET [2], and BET2 [30]. The comparative accuracy of the proposed approach versus the BSE, BET, and BET2 techniques on representative images for 3 subjects is shown in Fig. 3. As demonstrated in Fig. 3, our approach extracted the brain

Table 1. Comparative accuracy of our segmentation versus the methods in [2, 29, 30] by the DSC, MHD, and ABVD on 9 data sets with available ground truth ("M "– Mean and "SD "– standard deviation).

	Metric					
	DSC (%)		MHD (mm)		ABVD (mm^3)	
Method	M±SD	p-value	M±SD	p-value	M±SD	p-value
OUR	95.86±0.77	——	6.32±2.26	——	3.76±2.52	——
BSE [29]	93.17±1.44	0.0001	13.13±5.75	0.0007	5.64±2.11	0.0118
BET2 [30])	91.83±3.63	0.0049	13.80±6.74	0.0075	10.78±8.73	0.0137
BET [2]	91.80±3.42	0.0035	14.13±7.20	0.0099	10.58±8.33	0.0119

tissue more accurately compared with the BET and BET2 approaches. The lower performance of the BET [2] could be caused by its sensitivity to image noise and inhomogeneity, because this method relies only on voxels' intensity changes and does not account for spatial voxel interactions. On the other hand, the BET2 approach [2] slightly improves the brain extraction accuracy compared with the BET one. However, unlike the BET and our approach, the BET2 technique requires both T1-and T2-weighted MR images. Moreover, BSE [29] succeeds in accurately removing the skull but it removes small parts from the bain tissues as well, which may lead to inaccurate results for some clinical application (e.g. cortical thickness under-estimation). Table 1 compares our approach with the BSE, BET, and BET2, based on the DSC, MHD, and ABVD metrics for all the 9 data sets. As documented in Table 1, our approach performs notably better, according to its higher DSC and ABVD values and lower MHD value. Statistical significance of the better performance of our approach with respect to other methods is confirmed by the paired t-tests (p-values are less than 0.05).

In conclusion, this paper have introduced a novel framework for automated extraction of the brain from 3D infant MR images. Our experiments show that the fusion of first- and second-order visual appearance features of the MR brain data leads to more accurate brain extraction, when compared with widely-used brain extraction tools: BSE, BET, and BET2. The results were evaluated using the Dice similarity coefficient (DSC), 95-percentile modified Hausdorff distance (MHD), and the absolute brain volume difference (ABVD) on a cohort of 9 infant MR brain data sets.

6. REFERENCES

[1] A. J. van der Kouwe, T. Benner, D. H. Salat, and B. Fischl, "Brain morphometry with multiecho mprage," *Neuroimage*, vol. 40, no. 2, pp. 559–569, 2008.

[2] S. M. Smith, "Fast robust automated brain extraction," *Human brain mapping*, vol. 17, no. 3, pp. 143–155, 2002.

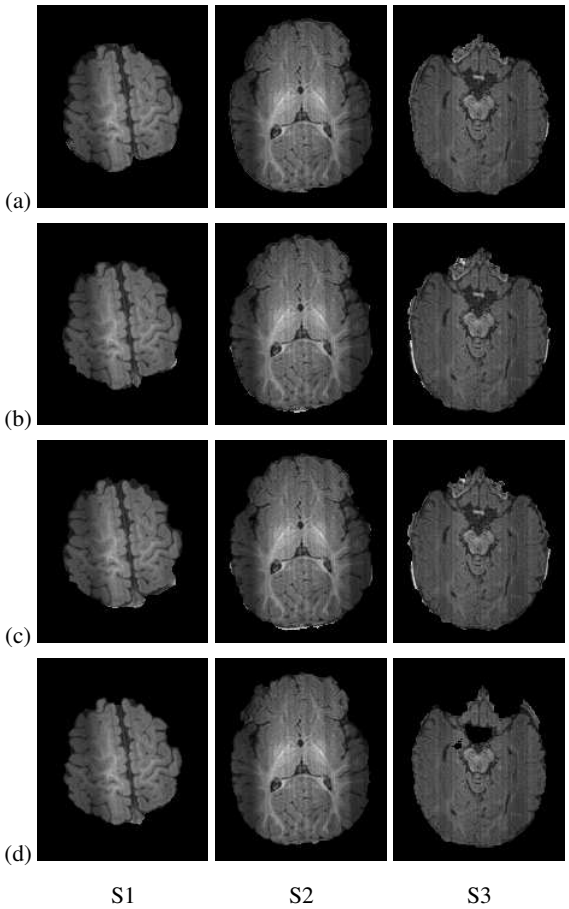

Fig. 3. Comparative results for three independent subjects (S1,S2,S3) using (a) our approach, (b) BET [2], (c) BET2 [30], and (d) BSE [29] approaches for three independent subjects.

[3] J.-X. Liu, Y.-S. Chen, and L.-F. Chen, "Accurate and robust extraction of brain regions using a deformable model based on radial basis functions," *Journal of neuroscience methods*, vol. 183, no. 2, pp. 255–266, 2009.

[4] A. H. Zhuang, D. J. Valentino, and A. W. Toga, "Skull-stripping magnetic resonance brain images using a model-based level set," *NeuroImage*, vol. 32, no. 1, pp. 79–92, 2006.

[5] J. Ashburner and K. J. Friston, "Voxel-based morphometrythe methods," *Neuroimage*, vol. 11, no. 6, pp. 805–821, 2000.

[6] K. K. Leung, J. Barnes, G. R. Ridgway, J. W. Bartlett, M. J. Clarkson, K. Macdonald, N. Schuff, N. C. Fox, and S. Ourselin, "Automated cross-sectional and longitudinal hippocampal volume measurement in mild cognitive

impairment and alzheimer's disease," *Neuroimage*, vol. 51, no. 4, pp. 1345–1359, 2010.

[7] J. E. Iglesias, C.-Y. Liu, P. M. Thompson, and Z. Tu, "Robust brain extraction across datasets and comparison with publicly available methods," *IEEE Transactions on Medical Imaging*, vol. 30, no. 9, pp. 1617–1634, 2011.

[8] F. Segonne, A. Dale, E. Busa, M. Glessner, D. Salat, H. Hahn, and B. Fischl, "A hybrid approach to the skull stripping problem in mri," *Neuroimage*, vol. 22, no. 3, pp. 1060–1075, 2004.

[9] D. E. Rex, D. W. Shattuck, R. P. Woods, K. L. Narr, E. Luders, K. Rehm, S. E. Stolzner, D. A. Rottenberg, and A. W. Toga, "A meta-algorithm for brain extraction in mri," *NeuroImage*, vol. 23, no. 2, pp. 625–637, 2004.

[10] D. W. Shattuck, G. Prasad, M. Mirza, K. L. Narr, and A. W. Toga, "Online resource for validation of brain segmentation methods," *NeuroImage*, vol. 45, no. 2, pp. 431–439, 2009.

[11] C. Fennema-Notestine, I. B. Ozyurt, C. P. Clark, S. Morris, A. Bischoff-Grethe, M. W. Bondi, T. L. Jernigan, B. Fischl, F. Segonne, D. W. Shattuck, et al., "Quantitative evaluation of automated skull-stripping methods applied to contemporary and legacy images: Effects of diagnosis, bias correction, and slice location," *Human brain mapping*, vol. 27, no. 2, pp. 99–113, 2006.

[12] F. Shi, Y. Fan, S. Tang, J. H. Gilmore, W. Lin, and D. Shen, "Neonatal brain image segmentation in longitudinal mri studies," *Neuroimage*, vol. 49, no. 1, pp. 391–400, 2010.

[13] A. U. Mewes, P. S. Hüppi, H. Als, F. J. Rybicki, T. E. Inder, G. B. McAnulty, R. V. Mulkern, R. L. Robertson, M. J. Rivkin, and S. K. Warfield, "Regional brain development in serial magnetic resonance imaging of low-risk preterm infants," *Pediatrics*, vol. 118, no. 1, pp. 23–33, 2006.

[14] A. Soliman, F. Khalifa, A. Alansary, G. Gimel'farb, and A. El-Baz, "Segmentation of lung region based on using parallel implementation of joint MGRF: Validation on 3D realistic lung phantoms," in *Proc.International Symposium on Biomedical Imaging (ISBI'13)*, 2013, pp. 852–855.

[15] M. Mostapha, A. Alansary, A. Soliman, F. Khalifa, M. Nitzken, R. Khodeir, M. F. Casanova, and A. El-Baz, "Atlas–based approach for the segmentation of infant DTI MR brain images," in *Proc. International Symposium on Biomedical Imaging (ISBI'14)*, 2014, pp. 1255–1258.

[16] N. J. Tustison, B. B. Avants, P. A. Cook, Y. Zheng, A. Egan, P. A. Yushkevich, and J. C. Gee, "N4ITK: Improved N3 bias correction," *IEEE Transactions on Medical Imaging*, vol. 29, no. 6, pp. 1310–1320, 2010.

[17] J. Besag, "On the statistical analysis of dirty pictures," *Journal of the Royal Statistical Society. Series B (Methodological)*, pp. 259–302, 1986.

[18] D. Adalsteinsson, *A fast level set method for propagating interfaces*, Ph.D. thesis, Citeseer, 1994.

[19] A. El-Baz, A. Elnakib, F. Khalifa, M. A. El-Ghar, P. McClure, A. Soliman, and G. Gimelrfarb, "Precise segmentation of 3-d magnetic resonance angiography," *IEEE Transactions on Biomedical Engineering*, vol. 59, no. 7, pp. 2019–2029, 2012.

[20] A. El-Baz and G. Gimel'farb, "EM based approximation of empirical distributions with linear combinations of discrete gaussians," in *IEEE International Conference on Image Processing, ICIP'07*. IEEE, 2007, vol. 4, pp. IV–373.

[21] A. A. Farag, A. El-Baz, and G. Gimel'farb, "Density estimation using modified expectation-maximization algorithm for a linear combination of gaussians," in *International Conference on Image Processing, ICIP'04*. IEEE, 2004, vol. 3, pp. 1871–1874.

[22] A. Farag, A. El-Baz, and G. Gimel'farb, "Precise segmentation of multimodal images," *IEEE Transactions on Image Processing*, vol. 15, no. 4, pp. 952–968, 2006.

[23] F. Khalifa, G. M. Beache, M. Abou El-Ghar, T. El-Diasty, G. Gimel'farb, M. Kong, and A. El-Baz, "Dynamic contrast-enhanced MRI-based early detection of acute renal transplant rejection," *IEEE Transactions on Medical Imaging*, vol. 32, no. 10, pp. 1910–1927, 2013.

[24] F. Khalifa, G. M. Beache, G. Gimel'farb, G. A. Giridharan, and A. El-Baz, "Accurate automatic analysis of cardiac cine images," *IEEE Transactions on Biomedical Engineering*, vol. 59, no. 2, pp. 445–455, 2012.

[25] A. El-Baz, *Novel stochastic models for medical image analysis*, Ph.D. thesis, University of Louisville, Louisville, KY, USA, 2006.

[26] "Infant brain imaging study (IBIS)," `http://www.ibisnetwork.org/`.

[27] D. LR, "Measures of the amount of ecologic association between species," *Ecology*, vol. 26, pp. 297–302, 1945.

[28] G. Gerig, M. Jomier, and M. Chakos, "Valmet: A new validation tool for assessing and improving 3d object segmentation," in *Medical Image Computing and Computer-Assisted Intervention (MICCAI'01)*. Springer, 2001, pp. 516–523.

[29] D. W. Shattuck and R. M. Leahy, "Brainsuite: an automated cortical surface identification tool," *Medical image analysis*, vol. 6, no. 2, pp. 129–142, 2002.

[30] M. Jenkinson, M. Pechaud, and S. Smith, "BET2: MR-based estimation of brain, skull and scalp surfaces," in *Eleventh annual meeting of the organization for human brain mapping*, 2005, vol. 17.